SPACE TELESCOPE SCIENCE INSTITUTE
Operated for NASA by AURA

Instrument Science Report STIS 2002-001

2-D Algorithm for Removing Scattered Light from STIS Echelle Data

Jeff A. Valenti, Don Lindler, Chuck Bowers, Ivo Busko, & Jessica Kim Quijano
July 23, 2002

ABSTRACT

Using the cores of saturated interstellar absorption lines, we demonstrate that a two-dimensional model of scattered light should be used when extracting STIS echelle spectra, particularly in the FUV where echelle grating scatter is significant. We describe the 2-D scattered light model of Lindler & Bowers, which includes the effects of echelle grating scatter, detector halo, telescope PSF, cross-disperser scatter, and ghosts. We also describe the algorithm developed by Lindler & Bowers to remove scattered light from STIS images by iteratively constructing a scattered light estimate from the extracted spectrum. Finally, we describe the implementation and performance of the Lindler & Bowers algorithm in the IRAF task x1d, which is part of the calstis spectral extraction package.

Ideally, a spectrograph should yield a one-to-one mapping between detector pixel and monochromatic source intensity. In practice, background, scattered light, and finite resolution contaminate the monochromatic signal in each pixel. Background subtraction and scattered light removal typically precede spectral extraction. Bias and dark subtraction removes the component of background that is independent of exposure level, leaving only the source spectrum and a component due to scattered light. For echelle spectrographs, one-dimensional linear interpolation of the minimum intensity between echelle orders provides a simple model of the scattered light beneath each order. Originally, this basic scattered light model was the only choice in the IRAF task **x1d** (McGrath et al. 1999), which is often used to extract echelle spectra obtained with the Space Telescope Imaging Spectrograph (STIS). Beginning with CALSTIS version 2.9 (installed in the archive pipeline on 2000 Dec 21 and released as part of STSDAS version 2.3 on 2001 June 12), **x1d**

also includes a new two-dimensional scattered light model *(algorithm = sc2d)* that supplements the original one-dimensional model *(algorithm = unweighted)*. This document describes the *sc2d* algorithm, developed by Lindler & Bowers (2001), implemented in CALSTIS by Busko, and tested by Valenti.

Several authors have suggested simple enhancements of the basic one-dimensional algorithm. For example, Howk & Sembach (2000) inferred the background beneath each order by fitting one-dimensional polynomials to an extended region around the minima between echelle orders. Alternatively, scattered light may be decomposed into a local one-dimensional component that scales with counts detected in the two immediately adjacent orders and a global two-dimensional polynomial component (e.g., Gehren & Ponz 1986; Hall et al. 1994; Churchill & Allen 1995). The formalism developed to interpret echelle data from the Goddard High-Resolution Spectrograph includes components that scale with total counts in an order and counts detected in each extracted wavelength bin (Cardelli et al. 1990; 1993). These one-dimensional components correspond to scatter by the echelle and the cross-disperser, respectively. In contrast to the models described above, the *sc2d* algorithm iteratively builds an empirical two-dimensional description of scattered light from one-dimensional extracted spectra and known scattering properties of the telescope and spectrograph.

Empirical Motivation

Development of a background subtraction algorithm (Lindler & Bowers 2001) with a two-dimensional scattered light model was motivated by unrealistic negative fluxes in saturated cores of interstellar absorption lines punctuating spectra of continuum sources. Figure 1 demonstrates the problem with extracted spectra obtained by subtracting either one-dimensional (1-D) or two-dimensional (2-D) estimates of the scattered light background. Hereafter, our discussion of the 1-D algorithm refers specifically to linear interpolation of interorder background, not the polynomial interpolation method of Howk & Sembach (2000). With the traditional 1-D background subtraction algorithm, the saturated line core is systematically below zero by 9.0 ± 0.4 % of the neighboring continuum flux. This must be an artifact of inadequate background subtraction. With the new 2-D scattered light model described here, the line core is only 1.0 ± 0.4 % below zero, indicating significant improvement.

Figure 2 presents a cut at column 500 (dashed vertical line) through the subimage shown in Figure 3. Echelle orders 330-338 are spaced nearly uniformly, except that order 334 is missing because of the strong interstellar line extracted in Figure 1. The *unweighted* algorithm in **x1d** estimates the background beneath each order by linearly interpolating the mean interorder light along columns. Order 334 (near row 640) is systematically below the 1-D background estimate (horizontal red line), indicating the need for a better method of estimating background.

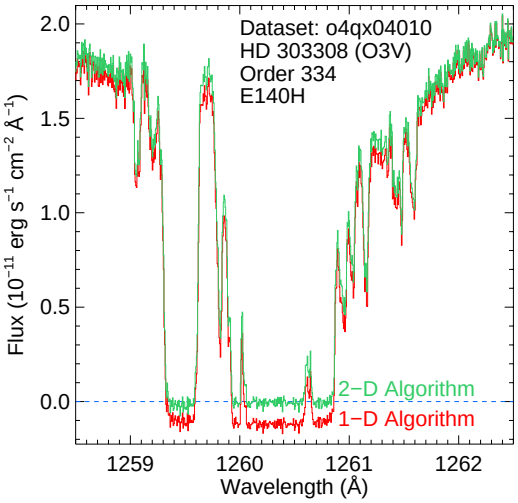

Figure 1: These interstellar absorption lines should have zero flux in the line cores, but extraction with a 1-D scattered light model yields negative fluxes.

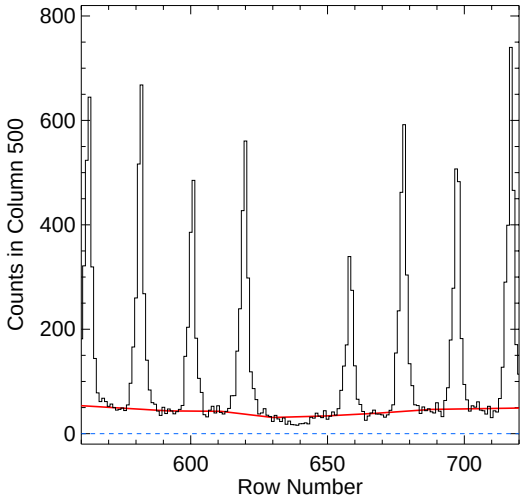

Figure 2: In this column cut across echelle orders, the deep absorption line in the order at row 640 drops below the 1-D scattered light model (red line).

Figure 3 shows a portion of a cross-dispersed echelle spectrum obtained in the FUV with the STIS E140H grating. The continuum of HD 303308 (black horizontal bands) is cut by interstellar absorption lines (white gaps) which should have zero signal in the final extracted spectrum. The image in Figure 3 has been clipped at 6% of the peak to highlight the behavior of the background. Note that absorption line cores are fainter (whiter) than the "background" between echelle orders. In this case, linear interpolation of interorder light along columns does not provide a good estimate of the background beneath an order.

Lindler and Bowers (2001) developed a 2-D algorithm (described below) which provides a better estimate of the background everywhere on the detector. Figure 4 shows the resulting 2-D background estimate for the subimage shown in Figure 3. The region around the strongest interstellar line complex is highlighted (dashed box) in both images. The background between orders is brighter (blacker) than the general background beneath each order, which in turn is higher than the faint background (white patches) beneath strong absorption lines. The 2-D algorithm yields a more realistic background model.

In Figures 3 and 4, the depressed background beneath strong absorption lines extends diagonally at a shallow angle with respect to detector rows. This shallow angle indicates the orientation of echelle grating scatter, as seen more clearly in Figure 5, which shows an E140H emission line spectrum of alpha Cen A (G2 V). Broad Ly-α emission with strong central absorption appears in echelle orders 346 (upper) and 347 (lower). The image has been clipped at 2% of the peak to highlight strong echelle scatter that diagonally connects Ly-α in two adjacent orders. Echelle scatter from Si III 1206.5 in order 349 is also visible.

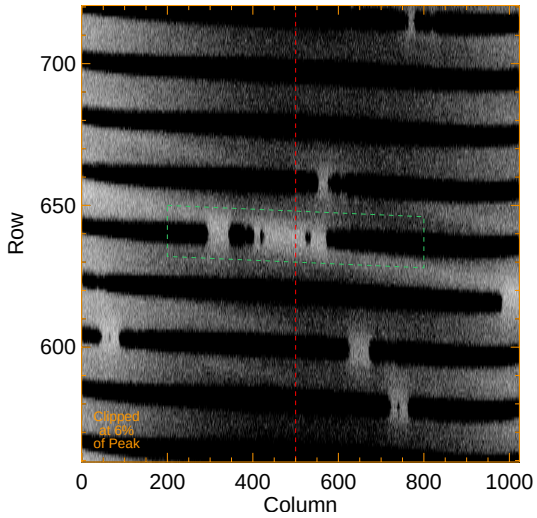

Figure 3: Counts in deep absorption lines are below (less dark) than the background between orders. A vertical line indicates the cut used in Figure 2.

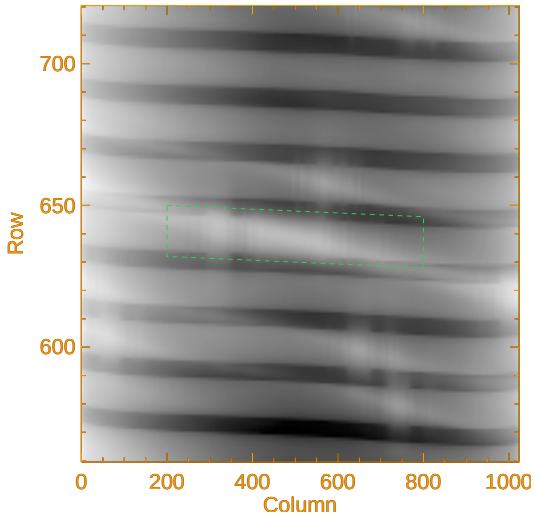

Figure 4: The 2-D scattered light model is lower (less dark) in the cores of deep absorption lines. A rectangle outlines the same regions as in Figure 3.

Figure 6 shows the extracted spectrum for order 346. Note how the 1-D algorithm actually *underestimates* the background in the absorption core of Ly-α, yielding errors about 1% of the peak flux. Near the right edge of Figure 6, the 1-D extraction goes negative because the diagonal echelle scatter visible in Figure 5 is crossing through the lower background region used to estimate background beneath order 346.

Algorithm Synopsis

In the Lindler and Bowers (2001) algorithm, a flat-fielded image is fitted with a 2-D model constructed in each iteration by folding the best current estimate of the extracted spectrum through a semi-empirical simulation of STIS optical properties. For STIS data, self-consistency between the model image and the extracted spectrum is achieved after three iterations. A 2-D scattered light model is then constructed considering only the echelle scatter outside an 11 pixel wide vertical window centered on each order. This 2-D scattered light model is subtracted from the original image, and the final spectrum is obtained using standard 1-D extraction. Key steps are described in more detail below.

1. Perform normal image processing to produce a flat-fielded count rate image, *IMAGE(x,y)*, as in Figure 7 (top left).
2. Perform spectral extraction with **x1d** to generate an extracted net spectrum versus wavelength, *NET(m,λ)*. Retain the *x* and *y* locations for each spectral order, *m*, and wavelength, λ, for construction of the model images from extracted spectra.

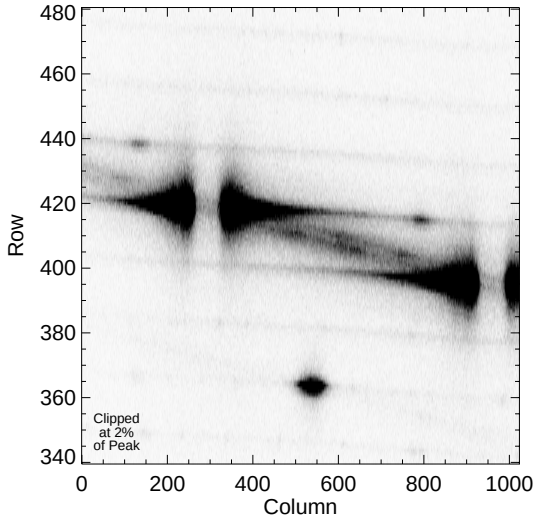

Figure 5: Echelle scatter connects the same double peaked Ly-α emission line in orders 346 (upper) and 347 (lower).

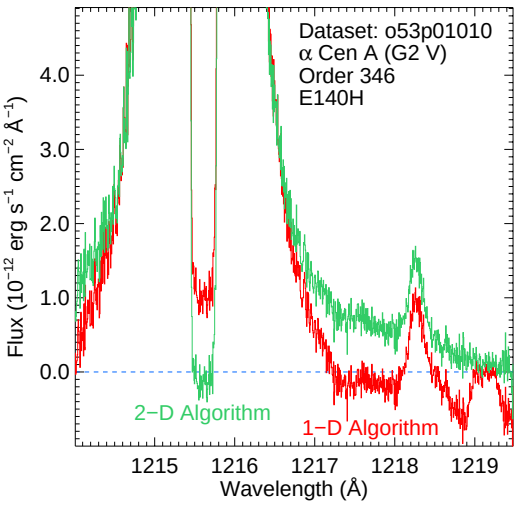

Figure 6: Extraction with 1-D model yields spurious positive flux in the core of Ly-α from row 420 of Figure 5.

3. Adopt *NET(m,λ)* as the initial estimate of the source flux distribution, *FLUX(m,λ)*.

4. Remove the echelle ripple function (Figure 8) from *FLUX*, and splice the spectral orders together to form a single spectrum vector, *F(λ)*.

5. Map the flux distribution *F(λ)* onto a over-sized model image, using the *x,y* locations as a function of m,λ from step 2 and extrapolated ripple functions.

6. Apply all forms of telescope, grating, and detector scattering (described below) to generate a model image, as in Figure 7 (top right)

7. Extract a new spectrum, *MOD_NET(m,λ)*, from the model image, using the same **x1d** parameters as in step 2.

8. Construct a new *FLUX* distribution, using a grating-dependent *Scale_factor* between 1.0 and 1.5 that controls the speed of convergence:

   *FLUX(m,λ) = FLUX(m,λ) + Scale_factor * (MOD_NET(m,λ) - NET(m,λ))*

9. Iterate steps 4-8 until convergence is achieved. Three iterations are adequate for all STIS echelle modes.

10. During the final iteration, also construct a 2-D scattered light image, *SCAT(x,y)*, using only the wings of the various scattering functions (described below). Figure 7 (bottom right) gives an example.

11. Construct a new image free of scattered light (Figure 7, bottom left) by subtracting the 2-D scattered light model from the original image:

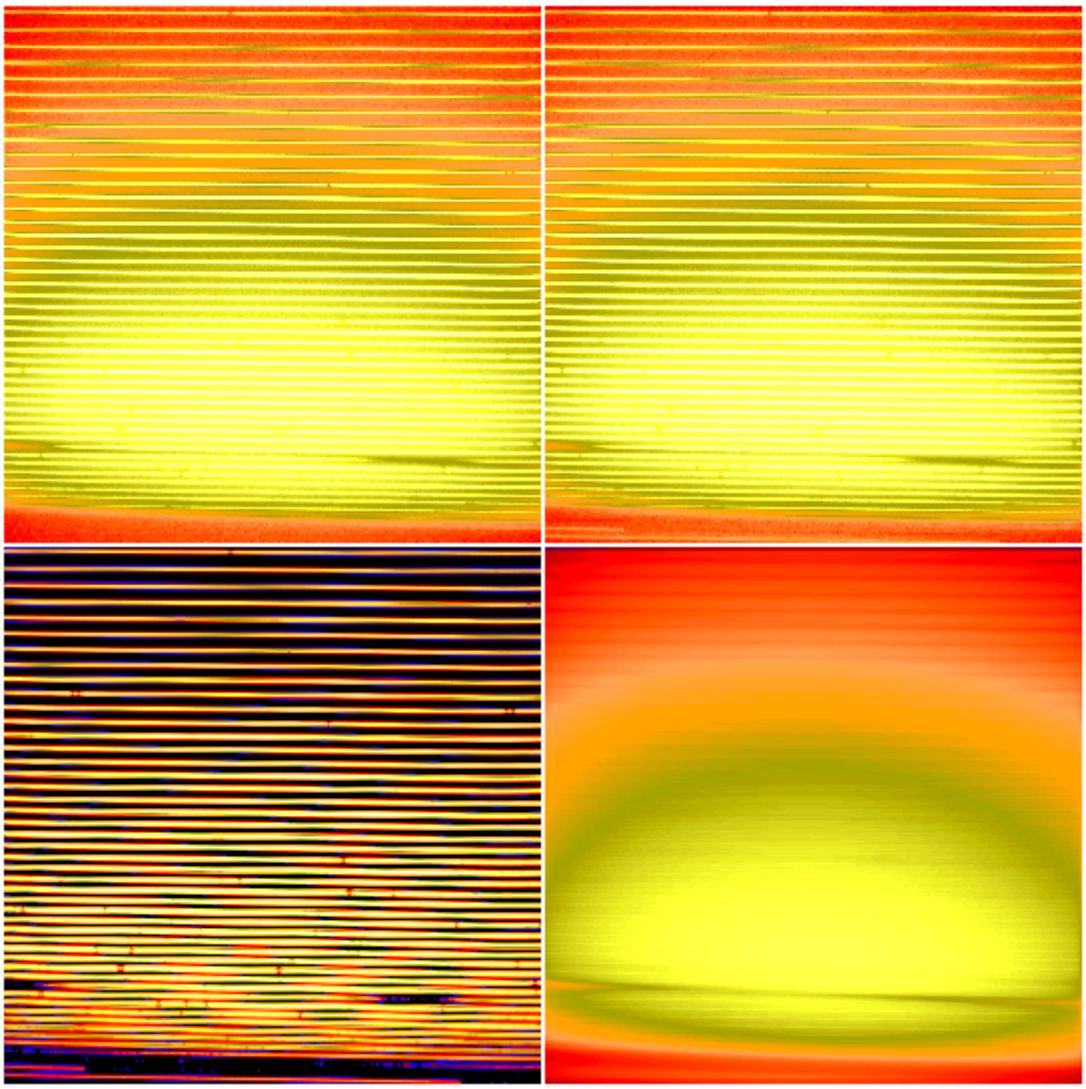

Figure 7: Model construction is illustrated for an absorption line source. *Upper Left:* E140M observation of BD+28 4211. *Upper Right:* model image generated self-consistently from an extracted spectrum and the adopted scattering model. *Lower Right:* scattered light portion of the model (constructed with the core of the PSF's and scattering functions removed). *Lower Left:* observed image (top left) minus the scattered light model (lower right), from which the final spectrum is extracted.

NEW_IMAGE(x,y) = IMAGE(x,y) - SCAT(x,y)

12. Extract the spectrum from *NEW_IMAGE* using **x1d** as in step 1. Interorder counts are still used to estimate and remove any residual scattered light and detector background not properly included in the model image (for example, light scattered from wavelengths not visible on the detector or the variable FUV detector glow).

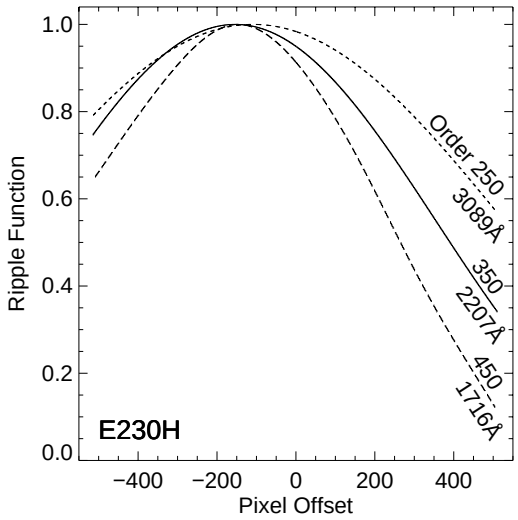

Figure 8: Echelle ripple (or blaze) functions (_rip) are used in constructing scattered light and image models from an extracted spectrum.

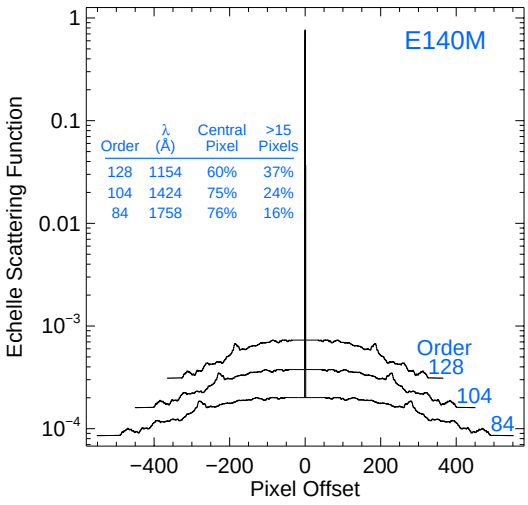

Figure 9: Echelle scatter (_ech) is modelled as a sharp core with broad wings. At short wavelengths, 1/3 of the light is scattered by more than 15 pixels.

Model Image Construction

In each iteration of the algorithm described above, a 2-D model is constructed by mapping extracted flux back onto an oversized model image and then numerically applying various scattering processes. The model image extends beyond the left and right edges of the physical detector to account for scattering contributions from the ends of orders not visible on the detector. Echelle scatter is modelled by redistributing extracted counts along diagonal lines of constant wavelength (e.g., Figure 5), using echelle line spread functions. Post-echelle smearing along columns is modelled by independently convolving each column with a scattering kernel. Scattering due to the aperture truncated telescope PSF, isotropic detector halo, and pre-echelle scattering by the cross-disperser are treated by 2-D convolution with a kernel constructed from these components. In the remainder of this section, we describe these scattering processes in more detail.

Scattered light from the echelle gratings is a significant contribution to STIS scattered light and is the main reason why a 1-D background model does not accurately reflect the scattered light beneath an order. Figure 9 shows echelle scatter functions for three orders of the E140M grating. A majority of the light is concentrated in the central pixel, but integrated light in the wings of the scattering function can be significant. At the shortest wavelengths, 37% of the light is scattered more than 15 pixels from the nominal position. As indicated in the table inset, scattered light increases dramatically at the short wave-

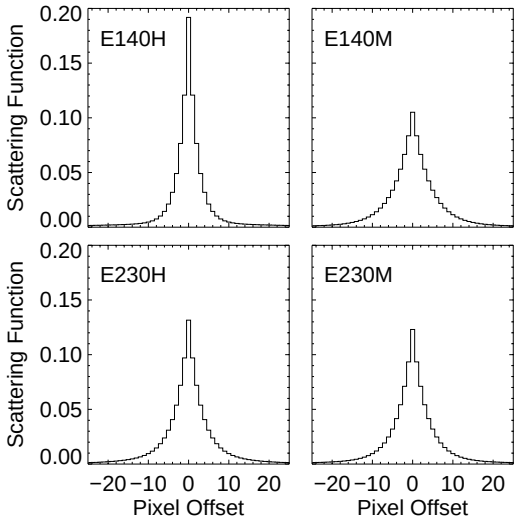

Figure 10: The broad component of the echelle scattering function in Figure 9 is also smeared in the cross-dispersion direction using depicted kernels (_exs).

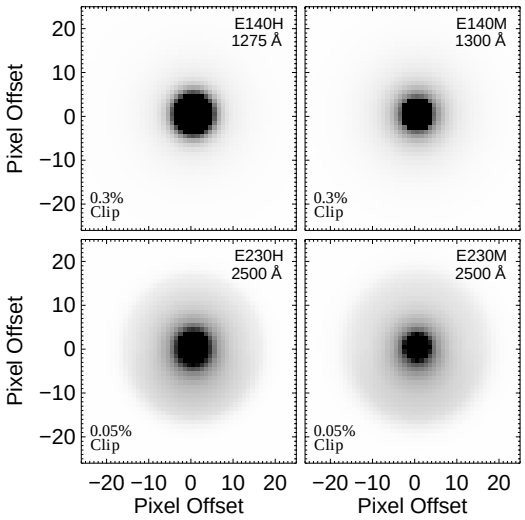

Figure 11: The 2-D scattered light model includes convolution with the detector halo kernel (_hal), which is more pronounced in the NUV.

length end of the FUV bandpass, presumably because the wavelength of incident light is becoming comparable to the size of irregularities on the reflection grating surface. At visible wavelengths, echelle scatter would be greatly diminished, reducing the need for a 2-D scattered light algorithm. The direction of the echelle scattering is approximately along the line connecting positions corresponding to the same wavelength in adjacent orders (see Figure 5), but there are small deviations. For the E140M and E140H modes, the deviations are roughly cubic with a maximum amplitude of about one pixel. Empirical distortion corrections for these two modes are included in the *sc2d* algorithm.

The broad wing component of echelle scatter (see Figure 9) is apparently subject to additional scattering in the cross-dispersion direction that does not affect light in the core of the scattering function. The cross-sectional shape of echelle scatter from an emission line is significantly broader than the cross-section of the emission line itself, indicating the presence of an additional scattering process. This implies the existence of an additional scattering process that applies only to the broad wing component of echelle scatter, not the core (see Figure 9). The scattering cannot be due to the cross-disperser, however, because cross-dispersers precede echelles in STIS. The physical origin of this empirically determined scattering contribution is not entirely clear. Figure 10 shows the broadening kernels that empirically reproduce the observed behavior of STIS. Widths of several pixels are consistent with the magnitude of the observed effect.

After including the effects of echelle scattering, the model image is convolved with a 2-D kernel to simulate the effects of the telescope PSF, detector PSF, and cross-disperser

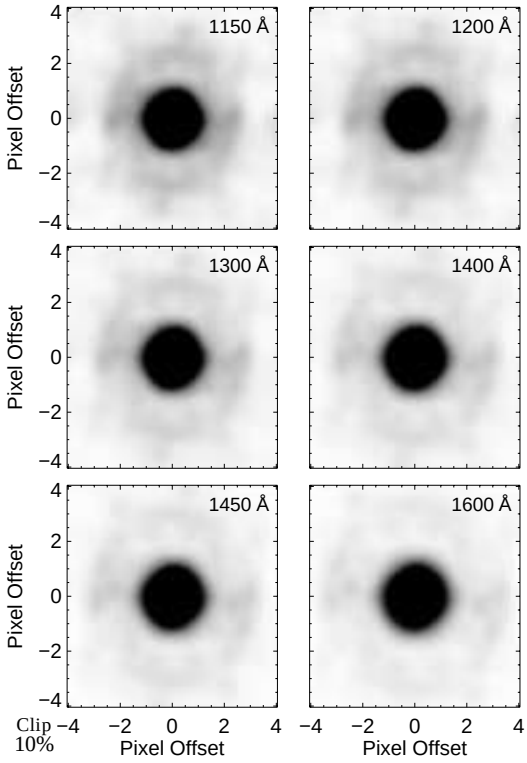

Figure 12: The 2-D scattered light model includes convolution with the wavelength dependent telescope PSF (_tel), clipped by the STIS aperture.

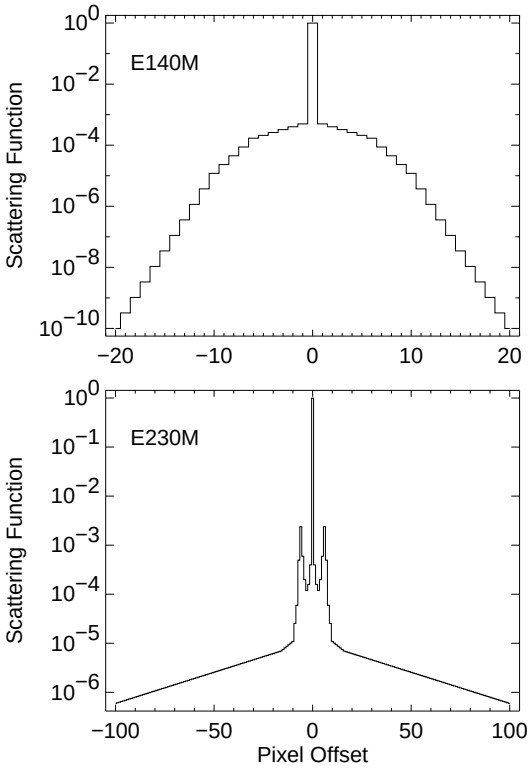

Figure 13: Cross-disperser scatter (_xds) is minor and included only for the sake of completeness. A δ-function is assumed for high resolution echelles.

scattering. Telescope and detector PSF can both change significantly with wavelength, corresponding to spatial variations in an echelle image, especially at shorter wavelengths. Rigorous convolution with a spatially varying PSF is not simple, but an approximate technique yields adequate results. The model image including echelle scatter is used to create a stack of one to three temporary images, each produced with a kernel appropriate for a different wavelength. A single model image is then formed by interpolating the stack of images as a function of the wavelength in each pixel of the output image. Outside the wavelength range spanned by the image stack, pixel values from the endpoint image are adopted, rather than extrapolating.

A calibration reference file (SRWTAB) contains the number and set of wavelengths used in constructing 2-D kernels. Figure 11 shows representative detector halo kernels, clipped to 0.3% or 0.05% of the peak to emphasize the wings. Note the prominent halo in the NUV-MAMA detector, which extends well into the interorder region. Figure 12 shows representative TIM models of the telescope PSF, clipped at 10% of the peak to emphasize the wings. Orientation of the telescope PSF remains fixed as viewed by STIS detectors.

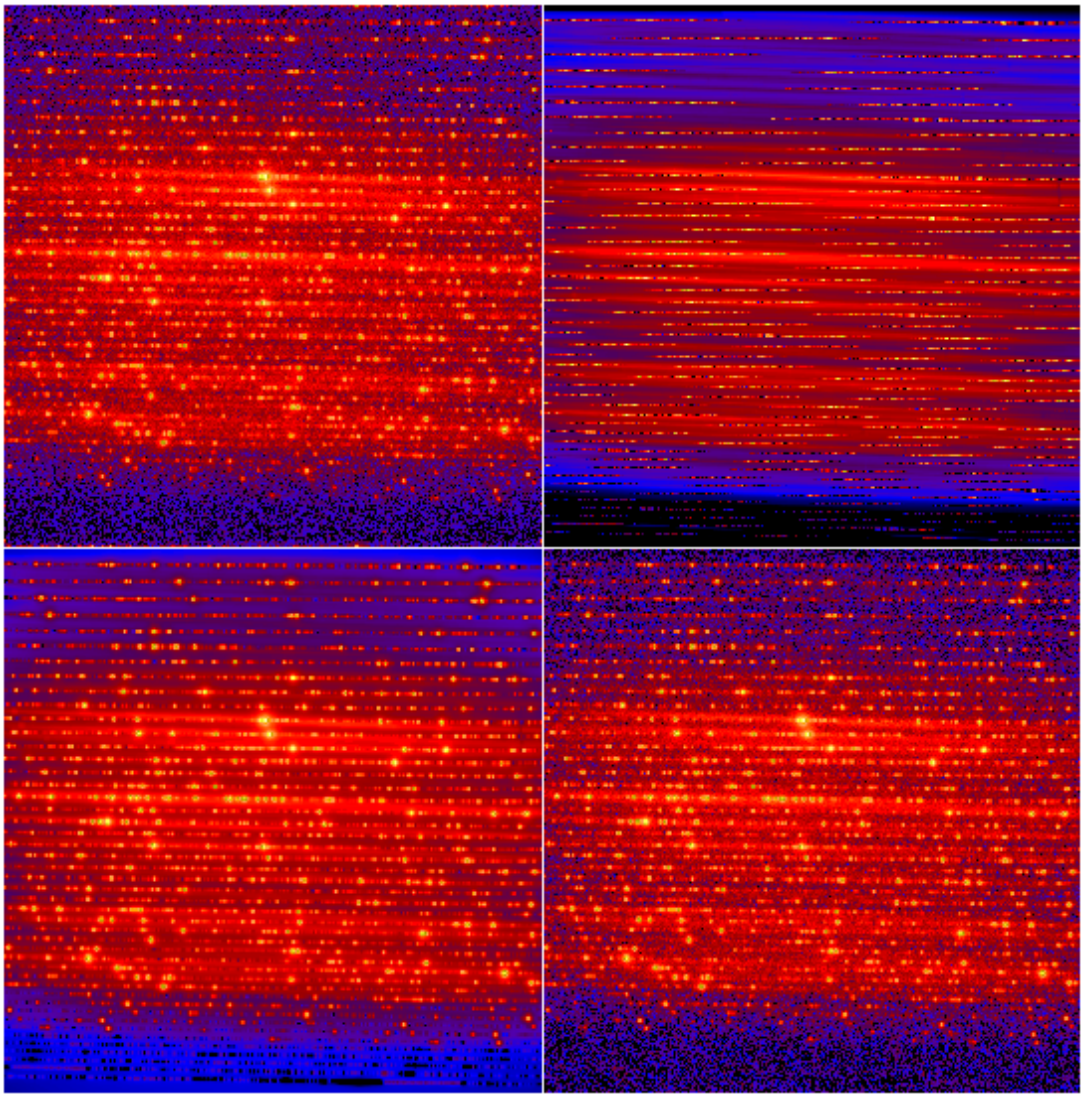

Model construction is illustrated for an emission line source. *Upper Left:* E140M observation of an emission line lamp. *Upper Right:* intermediate stage of model construction that includes only echelle grating scatter. *Lower Left:* final model after convolving the upper right image with the telescope, detector, and cross-dispersion PSFs. *Lower Right:* lower left image with Poisson noise (at the level in the observed data) added to visually match the texture of the observed image.

Only the portion of the PSF within the selected STIS aperture is used in construction of the model image. For lamp exposures, the STIS aperture is assumed to be uniformly illuminated, rather than using the clipped telescope PSF. After convolving the two PSFs together, the resulting kernel is convolved column-by-column with a cross-disperser scattering function, illustrated in Figure 13. This is a small contribution to the total scattered light, included only for the sake of completeness. In fact, the CDSTAB calibration refer-

Table 1: Reference File Types

FITS Keyword	File Suffix	Description
CDSTAB=	_cds	Cross Disperser Scatter
ECHSCTAB=	_ech	Echelle Scatter
EXSTAB=	_exs	Echelle Cross-Dispersion Scatter
HALOTAB=	_hal	Detector Halo
RIPTAB=	_rip	Echelle Ripple
SRWTAB=	_srw	Scattering Reference Wavelengths
PSFTAB=	_tel	Telescope Point Spread Function

ence file currently contains δ-functions for high resolution echelle gratings (E140H and E230H). Figure 14 illustrates a few stages of model image construction, using a spectrum of an emission line lamp.

Finally, ghosts due to window reflections are incorporated into the model image. A model ghost image is constructed by shifting, geometrically warping, and scaling the pre-ghost model image. The ghost image is smoothed because the ghost image is slightly out of focus due to a longer optical path. The ghost image shift depends on angle of incidence and hence position on the detector. For the E230M and E230H gratings, the ghost image is about 0.3% the intensity of the main image. Ghosts are negligible for the FUV detector.

STSDAS Implementation

The 2-D algorithm described above was first implemented by Lindler in IDL, taking advantage of the software and database environment maintained for the STIS Instrument Definition Team. Busko incorporated the algorithm into the existing **x1d** task in the IRAF package STSDAS. The **x1d** implementation is used in the archive pipeline and is supported for general use by the STIS community. Both the IDL and IRAF implementations have tasks named CALSTIS that drive end-to-end processing of STIS data, so an additional descriptor is required to distinguish between the two implementations (e.g., “the *sc2d* algorithm in the **x1d** task” uniquely specifies the IRAF implementation). The *sc2d* algorithm in **x1d** first appeared in CALSTIS version 2.9, which was installed in the archive pipeline on 2000 Dec 21 and released as part of STSDAS version 2.3 on 2001 June 12.

The 2-D algorithm requires a component level description of STIS optical properties, which Lindler and Bowers bundled into a variety of reference files. Implementation of the *sc2d* algorithm in **x1d** required the creation of 7 new reference file types, beyond those required for the original *unweighted* algorithm. Following the STSDAS convention, **x1d** obtains particular reference file names for each type from values corresponding to FITS header keywords ending in TAB. Reference files created at STScI have unique three letter

Table 2: Calibration Reference File Names and Sizes

Type	FUV Filename	Bytes	NUV Filename	Bytes
_cds	k8m09584o_cds.fits	8,640	k8m0958bo_cds.fits	8,640
_ech	k8m09585o_ech.fits	1,005,120	k8m0958co_ech.fits	1,823,040
_exs	k8m09586o_exs.fits	8,640	k8m0958do_exs.fits	8,640
_hal	k8m09587o_hal.fits	67,118,400	k8m0958eo_hal.fits	16,784,640
_rip	k8m09588o_rip.fits	4,320,000	k8m0958fo_rip.fits	10,497,600
_srw	k8m09589o_srw.fits	11,520	k8m0958go_srw.fits	17,280
_tel	k8m0958ao_tel.fits	933,120	k8m0958ho_tel.fits	624,960

suffixes that indicate the reference file type. Table 1 lists the header keywords and filename suffixes corresponding to the 7 reference file types used exclusively by the *sc2d* algorithm. Separate reference files exist for FUV and NUV modes. Table 2 gives the names and sizes of the **x1d** reference files created from the original Lindler and Bowers reference files. The two sets of reference files have identical content, but organization and FITS structure have been modified to match STSDAS conventions. If these reference files are modified in the future, careful testing will be required to assess the impact on behavior of the *sc2d* algorithm.

The STSDAS implementation of CALSTIS uses one other new keyword in the FITS header to control whether the original *unweighted* or new *sc2d* algorithm should be used to treat scattered light. If SC2DCORR is set to “PERFORM” in the _raw or _flt input file, then CALSTIS will invoke **x1d** with the *sc2d* option. This is currently the default behavior of the archive pipeline. If SC2DCORR exists and is set to “COMPLETE” in _x1d files created by **x1d**, then the spectrum was extracted using the *sc2d* algorithm. Data files retrieved from the HST archive prior to 2000 Dec 21 will not have the header keywords required to run the *sc2d* algorithm. An **sc2dref** script distributed with STSDAS may be used to update the headers of old data files, but in practice old data files should simply be replaced with new files from the HST archive, since the calibration data and software used in the pipeline steadily improves.

The difference between *sc2d* and *unweighted* extractions becomes less significant at longer wavelengths. Figure 15 compares extracted E140M spectra with a strong Ly-α absorption line that should have zero flux in the core. The measured flux in the line core is below zero by 9.2 ± 1.1 % in the *unweighted* extraction and by only 0.1 ± 0.4 % in the *sc2d* extraction. Figure 16 shows much smaller contrast for a Mg II line in the NUV, where the corresponding errors are only 0.6 ± 0.1 % and 0.1 ± 0.4 %. Figure 17 shows measured errors for these and other strong absorption lines, as a function of wavelength and echelle grating. Although the four echelle gratings could in principle have significantly different surface roughness, Figure 17 shows that 1-D extraction errors have a similar dependence

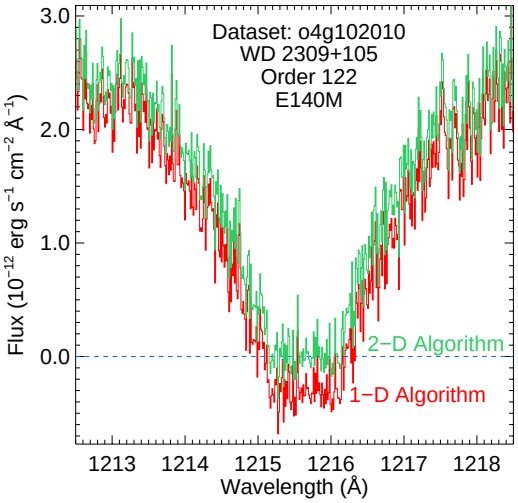

Figure 14: An E140M example demonstrating the improvement in line cores with the 2-D scattered light model.

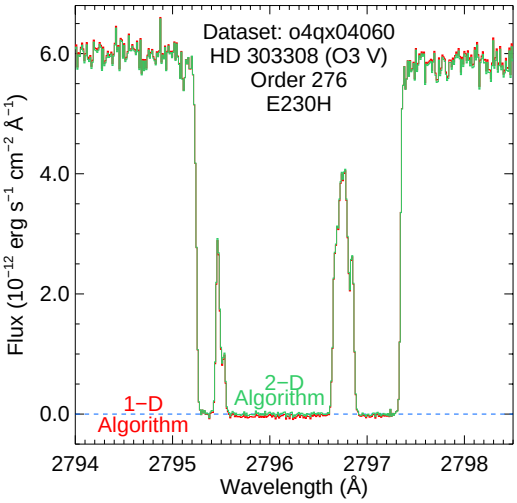

Figure 15: Both 1-D and 2-D algorithms perform similarly at long wavelengths, where echelle scatter is negligible.

on wavelength for all the echelle gratings. The factor of four increase in error from 1400 to 1100 Å, despite only a factor of two increase in echelle scatter over the same interval (table inset in Figure 9), may simply be due to the decrease in order spacing for bluer orders. This same effect could also account for the larger errors in E230H spectra at 1700 Å, relative to E140H spectra.

The **x1d** implementation of the *sc2d* algorithm was thoroughly tested against the IDL implementation and against *unweighted* extractions obtained with both packages. All four combinations of algorithm and implementation were used to extract 47 datasets covering 34 central wavelengths. The datasets included absorption and emission line spectra, and the full range of S/N ratio. Various test cases demonstrated proper behavior in *hires* pixel mode and for datasets containing multiple imsets.

Figure 18 shows the CPU time required to run **x1d** on the 47 test datasets, using the *sc2d* algorithm. Filled circles indicate single image datasets, whereas unfilled circles give averages for datasets with multiple imsets. Execution times generally decrease for settings with redder central wavelengths because there are fewer orders in each image and because fewer convolution kernels are required to adequately track the wavelength dependent PSF. When 3 kernel wavelengths are used, the executable image grows to 270 Mbytes, requiring 256 Mbytes of real memory to prevent debilitating swapping.

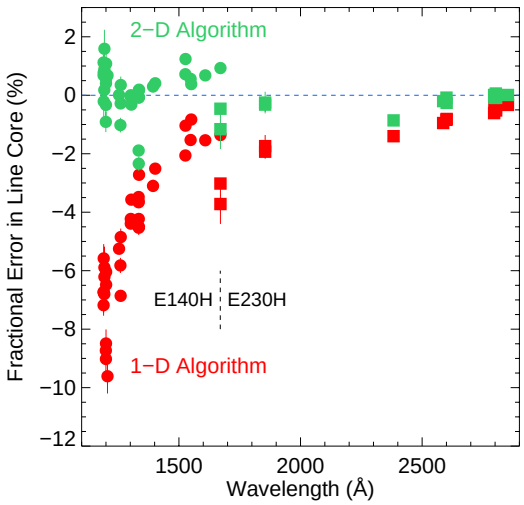

Figure 16: The cores of numerous deep absorption lines yield errors, relative to the local continuum and as a function of wavelength, for 1-D and 2-D models.

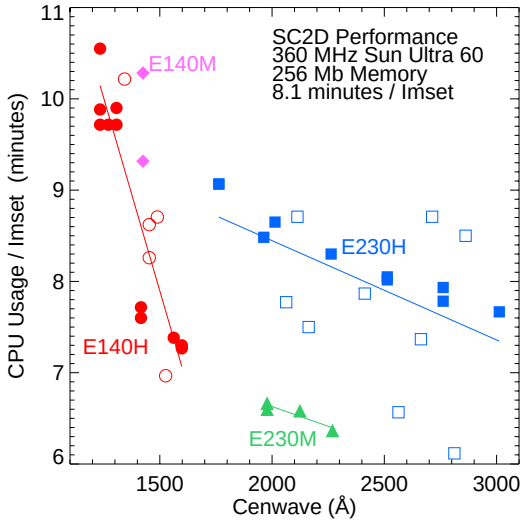

Figure 17: The 2-D algorithm involves convolution and iteration, using significant computer resources.

Acknowledgements

We thank Claus Leitherer and Ilana Dashevsky for early work on assessing 2-D scattered light models. We also thank Chris Howk for analyzing one of our test cases with his software.

References

Cardelli, J. A., Savage, B. D., & Ebbets, D. C. 1990, ApJ, 365, 789

Cardelli, J. A., Ebbets, D. C., & Savage, B. D. 1993, ApJ, 413, 401

Churchill, C. W., & Allen, S. L. 1995, PASP, 107, 708

Gehren, T., & Ponz, D. 1986, A&A, 168, 386

Hall, J. C., Fulton, E. E., Huenemoerder, D. P., Welty, A. D., & Neff, J. E. 1994, PASP, 106, 697

Howk, J. C., & Sembach, K. R. 2000, AJ, 119, 2481

Lindler, D., & Bowers, C. 2001, BAAS, 197.1202

McGrath, M. A., Busko, I., & Hodge, P. 1999, Instrument Science Report STIS 1999-03